Multiscale dynamics of helicity-dependent all-optical magnetization reversal in ferromagnetic Co/Pt multilayers

R. Medapalli,[1, *] D. Afanasiev,[2, 3] D. K. Kim,[1] Y. Quessab,[1, 4] S. Manna,[1] S. A. Montoya,[1] A. Kirilyuk,[2, 5] Th. Rasing,[2, 5] A. V. Kimel,[2, 5] and E. E. Fullerton[1]

[1]*Center for Memory and Recording Research, University of California San Diego, La Jolla, USA*
[2]*Radboud University, Institute for Molecules and Materials,*
Heyendaalseweg 135, Nijmegen, The Netherlands
[3]*Kavli Institute of Nanoscience, Delft University of Technology,*
P.O. Box 5046, 2600 GA Delft, The Netherland
[4]*Institut Jean Lamour, UMR CNRS 7198, Universite de Lorraine, Vandoeuvre-lès-Nancy, France*
[5]*Moscow Technological University, MIREA, Vernadsky Ave. 78, 119454, Moscow, Russia.*
(Dated: December 1, 2017)

Time-resolved magneto-optical imaging reveals that the dynamics of the helicity-dependent all-optical switching (HD-AOS) of Co/Pt ferromagnetic multilayers occurs on the timescales from nanoseconds to seconds. We find HD-AOS proceeds by two stages. First, for an optimized laser fluence, the ultrashort laser pulse demagnetizes the film to 25% of the initial magnetization. Subsequent laser pulses aids nucleation of small reversed domains. The observed nucleation is stochastic and independent of the helicity of laser light. At the second stage circularly polarized light breaks the degeneracy between the magnetic domains promoting a preferred direction of domain wall motion. One circular polarization results in a collapse of the reversed magnetic domains. The other polarization causes the growth of reversed magnetic domain from the nucleation sites, via deterministic displacement of the domain wall resulting in magnetization reversal. This mechanism is supported by further imaging studies of deterministic laser-induced displacement of the domain walls when excited by circular polarized optical pulses.

I. Introduction

Controlling the magnetic state of media with ultrashort laser pulses is a rapidly growing research area which promises to revolutionize information processing by achieving the fastest and least dissipative magnetic recording[1–4]. The mechanisms allowing femtosecond optical control of magnetism is a heavily debated fundamental question in ultrafast magnetism[5]. Recently, it was reported that in ferromagnetic Co/Pt multilayers the magnetization can be reversed upon excitation with a sequence of circularly polarized femtosecond laser pulses, where the final state is determined by the helicity of the laser pulses[6]. The mechanism developed earlier for ferrimagnets[7,8], based on the antiferromagnetic exchange between two sublattices, is not applicable in this case. Several mechanisms for the reversal in ferromagnets[9–15] have been proposed. In particular, Cornelissen *et al.*[13] suggested that the switching in Co/Pt multilayers can be realized by a single femtosecond laser pulse which acts as an ultrafast heater and a pulse of magnetic field. In contrast, based on time-resolved studies with millisecond temporal resolution, it was demonstrated[10,12,16] that the switching in ferromagnetic recording media requires multiple pulses. In the case of Co/Pt continuous multilayer films, it was reported theoretically[15] that the switching occurs via the formation of multiple laser-induced reversed magnetic domains. A repetition of this process results in merging of these individual reversed domains to form one single reversed domain. Similarly, very recently it was demonstrated that for a FePt nanoparticle recording medium, helicity-dependent all-optical switching can be explained by laser induced heating itself[9] or by an induced magnetization via the inverse Faraday effect[IFE][11] or in combination of both of them[10]. These debates raise questions about sub-100 ps magnetization dynamics triggered by a single laser pulse in the process of switching.

In this article, we present results of time-resolved magneto-optical experimental studies of both single-shot and multi-shot dynamics of helicity-dependent all-optical switching (HD-AOS) in a Co/Pt multilayer, starting from the ultrafast magnetic response to a single femtosecond pump pulse excitation to the formation and evolution of equilibrium reversed magnetic domains induced by multiple laser pulses. We have investigated the HD-AOS as a function of pump pulse duration, fluence, and repetition rate of circularly polarized ultrashort laser pulses. In this paper, we first determine the conditions for full magnetization HD-AOS in thin film Co/Pt multi-layers. Sweeping of the multi-pulsed laser beam along the sample surface revealed the optimal pulse duration and fluencies required for observing full magnetic reversal. The most efficient HD-AOS is achieved when the pulse length is longer than 2.0 ps. We present the ultrafast magnetization dynamics obtained from the single(4.0 ps pulse)-shot magneto-optical imaging. These results demonstrate that the nucleation of the reversed magnetic domain is stochastic and helicity-independent in nature. We further show that the multi-pulse induced full magnetization reversal obtained for various pulse-pulse delays within the range of 0.001-1 s. Our results visualize the dynamics of evolution of reversed magnetic domains during this multi-pulse excitation and reveals that the

helicity of the laser acts during the domain growth process. An analysis of the results shows that the initial displacement of the domain wall(DW) happens at a value of $\sim 50\,\mathrm{nm/pulse}$. We analyze the revealed trends in light of the magnetic circular dichroism and show that differential heating across the DW, separating oppositely magnetized domains, most likely causes the displacement of DW.

II.   Sample and experiment details

The sample studied is a multilayer stack of Ta(5 nm)/Pt(5 nm)/[Co(0.4 nm)/Pt(0.7 nm)]$_{x3}$/Pt(2 nm), grown by magnetron sputtering at an Ar pressure of 3 mTorr on a 500 µm thick double side polished soda lime glass substrate at a base pressure of 5 x 10^{-8} Torr. The film has strong perpendicular magnetic anisotropy, such that the two magnetic states emerge having magnetization oriented along or against the sample normal, $M^{\downarrow}$ or $M^{\uparrow}$, respectively. In our experiment we used a Ti:Sapphire amplified laser system producing Gaussian pulses at a central wavelength of 800 nm at a repetition rate of 1 kHz. The laser pulse duration was varied in the range of 0.1-4.0 ps using an internal grating-based pulse compressor and the corresponding full-width half maxima of the stretched pulse is measured using an external autocorrelator. The repetition rate of the laser pulses at the original wavelength was varied in the range 1-1000 Hz using a pulse picker synchronized with the laser source. This allowed us to vary the repetition period (P) of laser pulses within the range of 0.001-1 s. These pulses were used to pump the heterostructure in such way inducing magnetization reversal. The results presented in this paper are obtained from two different imaging experiments as described below.

In the first experiment, a halogen lamp was used as a light source to probe magnetic state of the sample. The sample was placed between two nearly crossed Glan-Taylor polarizers. The probe light guided through this optical path was collected by an optical objective and directed to the CCD matrix. This configuration allowed us to image magnetic domains via the magneto-optical Faraday effect with a resolution down to 1 µm. In the recording of magneto-optical images, the areas of the sample with oppositely oriented magnetizations are seen as black ($M^{\downarrow}$) and white ($M^{\uparrow}$) areas due to rotation of the probe polarization plane. The pump beam was incident at an angle of about 20° and focused into a spot of about 45 µm in diameter. The polarization of the pump pulses was controlled by a quarter wave retarder plate. A combination of optical half- wave retarder plate and a polarizer, in the path of pump beam, allowed a precise control of the pump laser fluence. The fluence of the pump pulses was estimated from the power, averaged for several seconds, using a power meter. The magneto-optical imaging of the sample magnetization was performed while the sweeping of the pump beam was done along the sample surface.

This allowed us to study the pump-pulse duration influence on the HD-AOS triggered by different repetition rates and durations of the pump pulses. The time resolution of this scheme is limited by the camera acquisition time being in our experiments close to 90 ms. To characterize the photo-induced state, the acquired images were digitized and integrals were taken over the areas where the magneto-optical contrast had been changed. The result of the integration, that represents the average net magnetization $\langle M \rangle$, is considered as a measure of the degree of switching in this paper. The case of $\langle M \rangle = 0$ corresponds to a multidomain state with zero average magnetization. The homogeneously magnetized domains with non-reversed or reversed magnetization correspond to $\langle M \rangle = -1$ and $\langle M \rangle = +1$, respectively.

In the second experiment, to study the sub-nanosecond magnetization dynamics triggered by a single pump pulse, a time-resolved single-shot magneto-optical imaging technique[17] was used. For this, a beam-splitter was placed at the output of amplifier to split the original laser beam into pump and probe pulses. Using a BBO crystal the probe pulses at a photon energy of 3.08 eV were generated via frequency doubling technique. A retro reflector placed on a motorized transnational stage was used to control the delay between pump and probe pulses. The probe beam was focused to larger area of about 300 µm and the angle of incidence was chosen to match the geometry employed for the magneto-optical imaging with halogen lamp described before. A single-shot pumping was achieved by placing a mechanical shutter in the path of the pump beam. The actuation time of the shutter was set to the lowest possible value of 60 ms. In order to exclude any possibility of excitation by more than one pump pulse, the repetition rate of the amplifier was brought down to 10 Hz. The camera exposure time was set to 1 ms. The activation time of the camera and the mechanical shutter were controlled by an external electrical delay generator synchronized with the laser. After each pump-probe event, the sample was brought to the initial single (magnetic) domain state by applying an external magnetic field of 1000 Oe, which is larger than the coercivity (H_C) in our sample (the room temperature H_C = 450 Oe). Note that the external magnetic field was set to zero before the pump pulse arrives on to the sample. Repeating such a single pump and single probe measurement for various time delays between a pump and a probe pulse, we reconstructed the laser-induced evolution magnetic domains. All the measurements were performed at room temperature. Throughout this paper, we discuss the results obtained when the sample was excited by either left-handed (σ^-) or right-handed (σ^+) circularly polarized laser pulses.
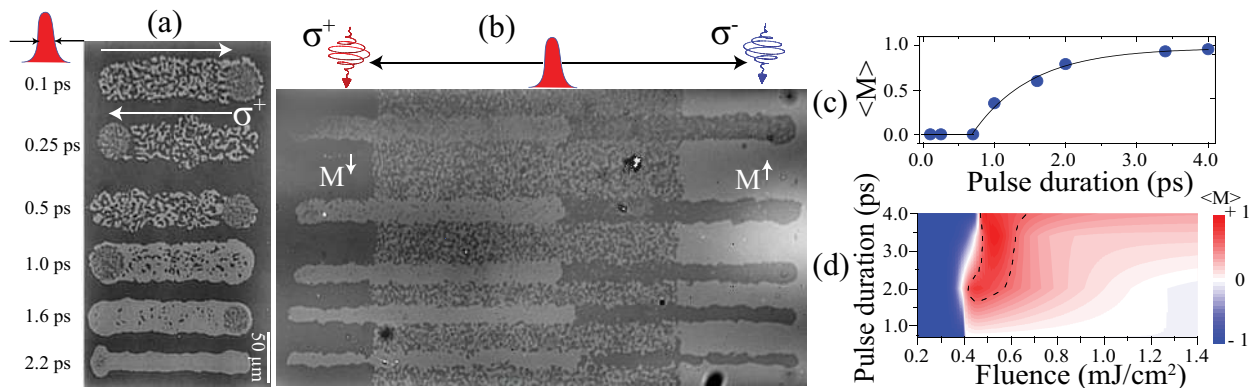
Figure 1. (a) Magneto-optical image of the multidomain patterns induced by sweeping of the circularly polarized pulsed laser beam along the sample surface. Each pattern corresponds to a specific duration of the pump pulse. The pump repetition rate is 500 Hz, laser fluence is $0.5 \, \text{mJ/cm}^2$. Arrows indicate direction of the sweep. (b) HD-AOS induced by a series of 4.0 ps optical pulses: Magneto-optical image of the domain patterns induced by slowly sweeping of the σ^+ (left)- and σ^- (right) circularly-polarized pulsed laser beam along the sample surface. The bright and dark regions represent $M^\uparrow$ and $M^\downarrow$-states, respectively. The multi-domain, demagnetized like, pattern between the uniform dark and bright regions was prepared by sweeping a 4.0 ps linearly (vertical)-polarized laser beam. After the sweeps, irrespective of the initial magnetic state, the final state is determined by the helicity of the laser pulses. The average laser-induced domain size increased with the increase in fluence, where the fluences used were 0.45, 0.5, 0.55, 0.6, and $0.7 \, \text{mJ/cm}^2$, respectively, from bottom to top. (c) Average value of the photo-induced magnetization ⟨M⟩ as a function of the pulse duration. The pump fluence and repetition rate is $0.5 \, \text{mJ/cm}^2$ and 500 Hz, respectively. (d) The phase diagram of the value ⟨M⟩ as a function of the pump pulse duration and fluence. The color bar indicates the value of ⟨M⟩. The dashed contour region shows the pump fluences and the pump pulse durations for which efficient switching was observed.

III.   Results

A.   Optimal conditions for multi-pulse induced helicity-dependent magnetization reversal in Co/Pt multilayers

To determine the optimal conditions for HD-AOS we used the static magneto-optical imaging technique, as described in Sec.II. Using this we recorded the magneto-optical images after the sweeping of the laser beam along the sample surface was done. The laser swept regions were exposed to a 500 Hz pulsed laser beam moving at a speed of $1 \, \mu\text{m/s}$, which allowed nearly 500 pump pulses excitations per every $1 \, \mu\text{m}$ region on the sample. We repeated this experiment as a function of pump pulse duration in the range of 0.1-4.0 ps and fluence in the range of 0.2-$1.4 \, \text{mJ/cm}^2$. The results for 0.1-2.2 ps are shown in Fig. 1a. The fluence dependence of helicity-dependent all-optical switching obtained by sweeping a sequence of 4.0 ps laser pulses is shown in Fig. 1b. The pulse duration dependence of the degree of the magnetization reversal (see Fig.1c) and the color mapping (see Fig. 1d) of the fluence dependence and pulse durations clearly demonstrate that the HD-AOS is the most efficient when the pulse duration is 2.0 ps or above and a fluence near $0.5 \, \text{mJ/cm}^2$. The observed multi-domain pattern at a fluence of $0.6 \, \text{mJ/cm}^2$ or above for a 4.0 ps laser pulse is very similar to what has been observed for the lower fluences ($0.5 \, \text{mJ/cm}^2$) of 100 fs laser pulses. This is due to the fact that even the longer pulses induce a higher degree of demagnetization at higher fluences. This observation that longer pulse lengths result in more efficient reversal when sweeping the beam is consistent with the results for TbCo films[20].

B.   Ultrafast laser-induced magnetization dynamics obtained from time-resolved single shot imaging
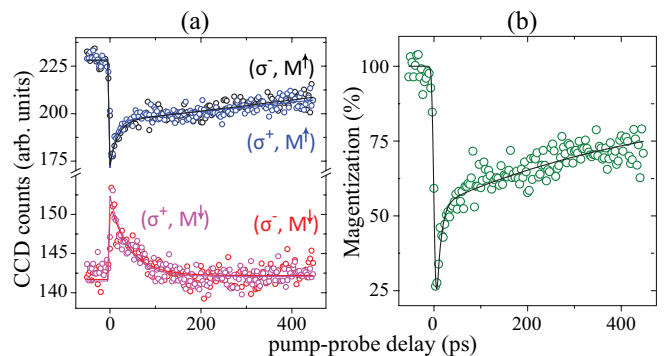

Figure 2. (a) The single-shot dynamics of the average value of the magneto-optical contrast in the area affected by the pump pulse for different combinations of the light helicity (σ^-, σ^+) and magnetic ground state ($M^\downarrow$, $M^\uparrow$). (b) The dynamics of the absolute demagnetization. The pump fluence is $0.5 \, \text{mJ/cm}^2$, the pulse duration is 4.0 ps. The solid lines are the double exponential function fits to the experimental data.

To determine the effect of a single pump pulse and to reveal if any helicity-dependent dynamics is present in the sub-ns time-domain, a time-resolved experiment, for two opposite helicities (σ^-, σ^+) of the pumping light and two initial states of the magnetization ($M^\downarrow$, $M^\uparrow$) was performed. For this, an optimal combination of duration(4.0 ps) and fluence (0.5 mJ/cm^2), obtained from the multiple pulse (at 500 Hz) excitation measurements shown in Fig. 1 was used. For this combination of pulse duration, fluence and helicity we obtained fully deterministic all-optical switching when the laser was swept over the sample. Thus, we used these laser parameters to explore the ultrafast response. The magnetization dynamics for each of the combinations of pump helicity and initial magnetization is plotted in Fig.2a. One can clearly see that the laser excitation results in a rapid partial demagnetization, followed by a recovery. Interestingly, changing the helicity of the pump light does not result in any pronounced difference in the sub-ns photo-induced dynamics. The asymmetry in the signals for two opposite values of the magnetization as seen in Fig. 2 originates from the intrinsically nonlinear response of the cross-polarized magneto-optical imaging technique[19]. One may argue that the non-linearity can be avoided by opening the analyzer further. This will increase the signal, but decrease signal-to-noise ratio making the measurements impossible. Even if one neglects the noise of the light source assuming that the shot-noise is dominating, it is easy to show that the noise will scale as a square root of the light intensity at the CCD camera. Hence, the best signal-to-noise ratio is expected when the polarizer and the analyzer are nearly crossed. To eliminate the non-linearlity in our experiments, and to obtain quantitative values of the demagnetization, the difference was taken and normalized value to the level of magneto-optical contrast achieved for the two fully saturated oppositely magnetized states of the sample. The corresponding value is proportional to the net magnetization in the probed region. The laser-induced ultrafast magnetization dynamics is plotted in Fig.2b. It is seen that the ultrafast demagnetization for this pump fluence of 0.5 mJ/cm^2 reaches 75 %. The subsequent magnetization recovery takes more than 500 ps and demonstrates a double exponential relaxation, similar to that observed in Ref.21. The characteristic relaxation time extracted from the fit, shown in Fig.2b, is 500 ps. Hence, these experiments emphasize the importance of multiple pulse excitation as is not observed for a single pulse even though full reversal was observed sweeping the beam.

IV. Multi-pulse induced magnetization dynamics

To investigate how multiple-pulse excitation leads to magnetization reversal, we exposed the sample to a sequence of 4.0 ps laser pulses at various repetition rates ranging from 1-1000 Hz, having the pump spot at a fixed position on the sample. This resulted in helicity-dependent full magnetization reversal and the corresponding dynamics are shown in Fig.3 for the case of 1 kHz. The photo-induced changes for various exposure times (up to 50 s) are shown in Fig.3a for all the four combinations of (σ, M). The dashed circle in Fig.3a represents the laser-irradiated region. In order to show the evolution of reversed magnetic domain from the nucleation cites, we obtained the cross-sections at the center of the laser excited region (see dashed line in Fig.3a). The corresponding line profiles are merged together as a sequence of exposure time and shown, in Fig.3b, for both shorter and longer exposition time scales. Note the presence of reversed nucleation sites even in the cases ((σ^-, $M^\downarrow$) and (σ^+, $M^\uparrow$)) where the magnetization reversal
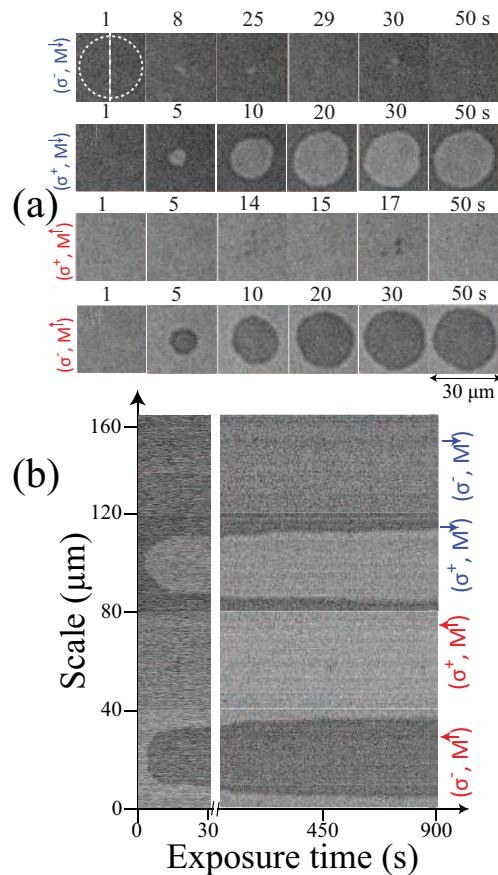

Figure 3. (a) Magneto-optical images of the laser-induced magnetic domains, taken at various exposition times, when subjected to the repetitive action of the pump pulses with the frequency of 1 kHz for a pump fluence of 0.5 mJ/cm^2. The number on each image shows the exposition time at which it was recorded. b) The reversed domain size as a function of exposure time. Plotted are vertical cross-section obtained along a line cross-section shown in a) at the center of the laser-excited area for different combinations of initial saturated magnetization states ($M^\downarrow$ or $M^\uparrow$) and helicity of circularly polarized pump pulses (σ^- or σ^+). The pump fluence per pulse and its repetition rate are 0.5 mJ/cm^2 and 1 kHz, respectively. Note that the growth and the orientation of the magnetization direction are determined by the helicity.

does not take place. Clearly, the growth or the reduction of the nucleated domains is determined by the helicity of the laser pulses.

The photo-induced changes in the region exposed to the repetitive action of the laser pulses at the rate of 1 Hz for various time intervals are shown in Fig.4a for the $(\sigma^-, M^\uparrow)$ combination. The first visible changes in the magnetic contrast appear only after 60 s, i.e. when the sample has already been excited by 60 pulses. However, the number of pulses needed for nucleation is stochastic and can vary when the experiment is repeated. The evolution of the domains for various P values, obtained from line scans across the center of the illuminated area as shown in Fig. 4a, are shown in Fig. 4b. The net change in magnetization ΔM in the direction of the propagation light, normalized to the $\langle$M$\rangle$ values obtained from the image taken before the arrival of the pump pulse, is defined as ΔM/$\langle$M$\rangle$. The obtained values of ΔM/$\langle$M$\rangle$ along a line cross-section (see Fig. 4a) at the center of the laser-excited area for the combination of $(\sigma^-, M^\uparrow)$ are plotted as a function of exposure time, and are shown in Fig.4c. The various curves correspond to the net magnetization reversal dynamics obtained for various Ps of pump laser pulses. In all the cases the multi-pulse dynamics is described by nucleation followed by a gradual growth of the reversed domain. The exposure time required to form a reversed magnetic domain with a diameter of 18 μm is obtained using single exponential fits to the ΔM/$\langle$M$\rangle$ data for various P and is plotted in Fig. 5, showing a distinguished linear dependency at a threshold, P = 0.01 s. Note that the required exposure time varies with the length of cross-section lines chosen at the center of the laser-exposed regime. The slope of the line linear fit, in turn, reveals the number of pulses necessary to accomplish the full reversal of a magnetic domain with a diameter of 18 μm. It is ∼600 pulses for $P\geqslant0.01$ s regime. However, for the $P\leq0.01$ s it is nearly 2000 pulses.

It is known that magnetzation reversal is a first-order phase transition[23]. In the kinetics of such phase transitions one distinguishes two regimes: nucleation of the domains of the new phase and their subsequent growth. To study these two regimes more in detail, we first exposed the sample to a sequence of 660 pulses with a pulse duration of 4.0 ps and a repetition rate of 1 Hz, while the conditions of the beam helicity and the magnetization were fixed either to $(\sigma^-, M^\uparrow)$ or $(\sigma^+, M^\downarrow)$, for which we observed full magnetization reversal. The photo-induced changes for various exposure times are shown in Fig. 6a. For the $(\sigma^+, M^\downarrow)$ case, first visible changes in the magnetic contrast appear only after 20 s, i.e. when the sample has already been excited by 20 pulses, whereas in the $(\sigma^-, M^\uparrow)$ case it is at 5 s. The number of pulses required to nucleate a reversed domain as well as the number of nuclei varied when the experiment was repeated. Figure 6a clearly shows that for the case where multiple domains are nucleated, the domains first grow with no visible mutual correlations before merging into a single domain after ∼150 s for both $(\sigma^-, M^\uparrow)$ and $(\sigma^+, M^\downarrow)$. From this

stage, the reversed domain grows further radially until reaching its equilibrium size, at which the growth of the laser-induced reversed magnetic domain stops. The latter is defined by the pump spot size and fluence. For a given fluence of 0.5 mJ/cm^2, after 660 pulses, a reversed magnetic domain with a diameter of 11±1 μm is formed.

The values of ΔM/$\langle$M$\rangle$ acquired from the center of the laser excited region (dashed circle ($\varnothing$ = 11 μm) in Fig. 6a) are plotted as a function of exposure time, and are shown in Fig. 6b. Note that the data shown is obtained from the average of several measurements [see Fig.7]. The insets in Fig. 6b show the initial ΔM/$\langle$M$\rangle$ dynamics for both the the $(\sigma^-, M^\uparrow)$ and $(\sigma^+, M^\downarrow)$ cases up to 30 s of exposure time. The observed laser-induced dynamics shown in Fig.6b shows a fast decrease and subsequent reversal of ΔM/$\langle$M$\rangle$ with a saturation towards the final reversed state at longer exposure times. The initial growth rate of ΔM/$\langle$M$\rangle$ until ∼150 s corresponds to the growth and final merging of the individual nuclei into a single magnetic domain. The solid curves in Fig.6b are the fits, to the exposition interval 150-660 s, obtained using a single exponential function. The subsequent ΔM/$\langle$M$\rangle$ dynamics corresponds to the growth of the thus formed domain under the action of the circularly polarized pump pulses. To quantify these growth rates we took the $\sqrt{\Delta M/\langle M\rangle}$ values from the fits shown in Fig.6b and normalized the obtained radii to the final diameter of 11 μm experimentally observed at 660 s. The results are shown in Fig.6c for both $(\sigma^-, M^\uparrow)$ and $(\sigma^+,$
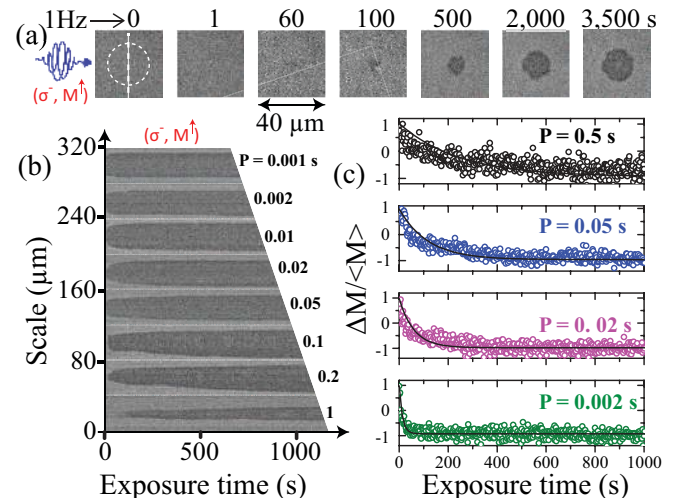

Figure 4. a) Magneto-optical images of laser-induced magnetic domains subjected to the repetitive action of the pump pulses $(\sigma^-, M^\uparrow)$. The repetition rate is 1 Hz. The pump fluence is 0.5 mJ/cm^2, and the pulse duration is 4.0 ps. (b) The magnetization dynamics in a cross-section of the laser-excited area for different repetition rates. (c) The net magnetization dynamics obtained along a line cross-section (see Fig. 2a) at the center of the laser-excited area for the combination of $(\sigma^-, M^\uparrow)$. The various curves correspond to the ΔM/$\langle$M$\rangle$ dynamics obtained for various Ps of pump laser pulses. The fluence is 0.5 mJ/cm^2.
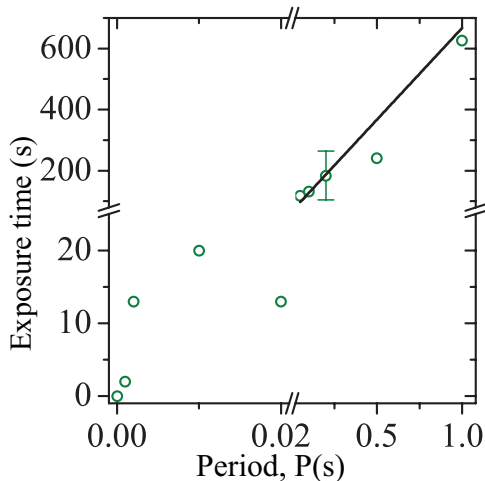
Figure 5. The characteristic exposure time at which a magnetic domain with a diameter of $18\,\mu m$ is formed is plotted against the repetition period, P. The straight lines are linear fits to the data.

$M^{\downarrow}$) cases. From the derivative of the radius as a function of exposure time we can obtain the growth rate of the reversed domain. This rate is also plotted, as displacement(D) per pulse, in Fig.6c. For the initial period of 0-150 s, we find an average growth rate of $\sim 200\,nm/pulse$, which corresponds to the growth and collapse of the individual nuclei to a single domain. For the subsequent period 150-600 s, the growth corresponds to the displacement of the DW separating the reversed domain from the surrounding initial magnetization direction. This displacement per pulse starts at about $50\,nm/pulse$ for both $(\sigma^{-}, M^{\uparrow})$ and $(\sigma^{+}, M^{\downarrow})$ cases, and decreases asymptotically to $0\,nm/pulse$ for times approaching $660\,s$ for the selected $11\,\mu m$ circular region.

V. Discussion

Our experimental results thus visualize a two step mechanism of helicity dependent optically induced magnetization reversal: a helicity-independent demagnetization and nucleation of reversed domains, and a subsequent helicity-dependent coalescence and growth of the reverse domain due to laser induced DW motion. The helicity dependence of this laser induced domain wall motion is independently studied and is visualized in Fig.8. Figure 8a shows the images of the $M^{\uparrow}$ and $M^{\downarrow}$-regions, separated by a DW, taken before and after exposure to a sequence of 100, 600, and 3,600 circularly-polarized laser pulses. In these experiments the beam intensity was lowered to $0.4\,mJ/cm^{2}$ which is below the fluence to achieve HD-AOS as seen in Fig.1. The displacement of the DW, under σ^{-}-excitation, towards the $M^{\uparrow}$-region is clearly visible in the top row images of Fig. 8a. The bottom row shows a similar result, for the case of σ^{+}-pulses, with the DW displacing in the opposite direction,
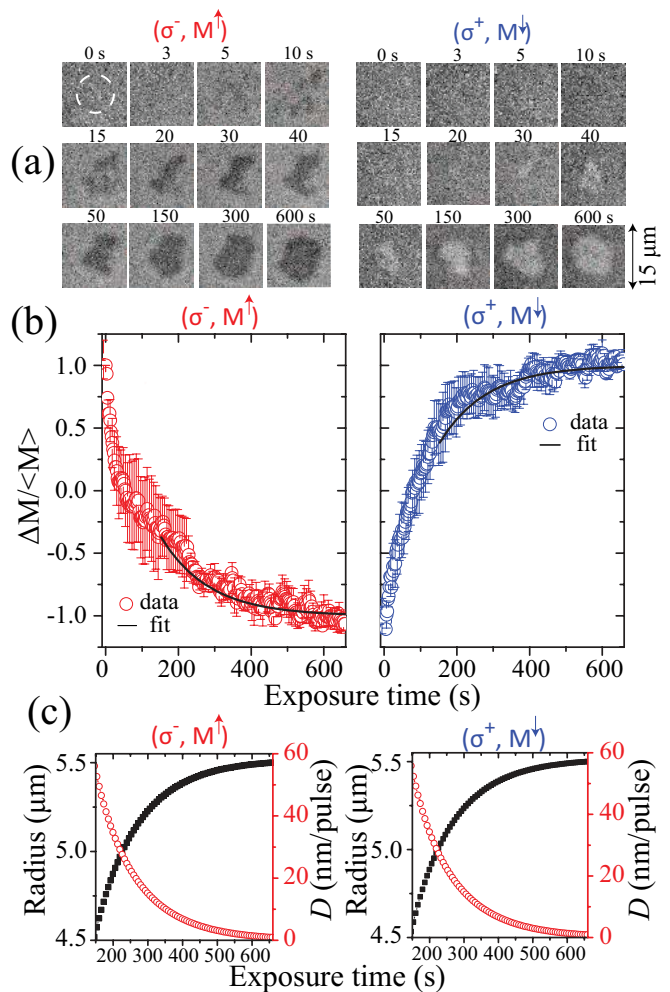

Figure 6. (a) Magneto-optical images of the laser-induced magnetic domains, taken at various camera exposition times, when subjected to the repetitive action of the pump pulses are shown for (left) $(\sigma^{-}, M^{\uparrow})$, and for (right)$(\sigma^{+}, M^{\downarrow})$. The repetition rate is $1\,Hz$, the pump fluence is $0.5\,mJ/cm^{2}$. (b) The net magnetization dynamics observed at the center of laser-excited area for both (left) $(\sigma^{-}, M^{\uparrow})$ and (right) $(\sigma^{+}, M^{\downarrow})$ cases. The error bars represent the standard deviation in the measurements. The solid black curves are single exponential function fits to the data. (c) (left) The dynamics of radius of the reversed magnetic domain and displacement per pulse, during growth of the reversed magnetic domain, for $(\sigma^{-}, M^{\uparrow})$ and (right) $(\sigma^{+}, M^{\downarrow})$ are shown. Note that to quantify these growth rates we took the $\sqrt{\Delta M / \langle M \rangle}$ values from the fits shown in (b) and normalized the obtained radii to the final diameter of $11\,\mu m$ experimentally observed at 660 s.

i.e. towards the $M^{\downarrow}$-region. The displacement/pulse values within 0-100, 100-600, and 600-3600s are 45, 11, and $\sim 2\,nm$, respectively. The direction of DW displacement is clearly linked to the helicity of the excitation and hence provides an insight into the fundamental mechanism of HD-AOS in these ferromagnetic multilayers. If one assumes that the upper limit for the DW speed in thin
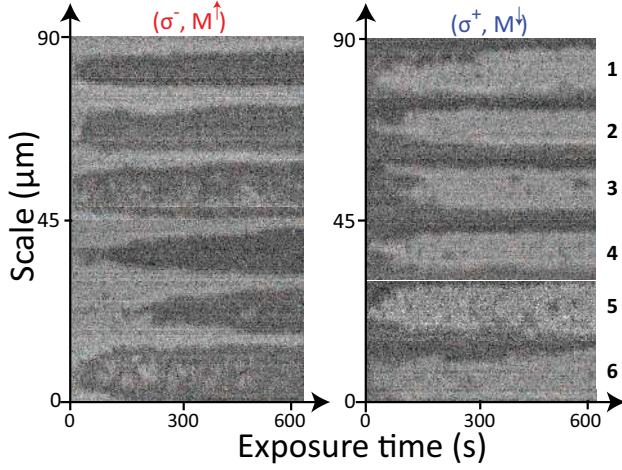
Figure 7. Magneto-optical images of the domain patterns induced by repetitive excitation of σ^- (left), σ^+ (right) circularly-polarized pulsed laser beam on a homogeneously magnetized regions along $M^\uparrow$ (left), and $M^\downarrow$ (right). Images are obtained by merging the cross-sections at the center of the laser excited region, imaged after each pulse. Note that the merging is done as a sequence of exposure time. Each laser-induced magnetic domain pattern corresponds to 4.0 ps duration pump pulses with a repetition rate of 1 Hz, and a fluence of 0.5 mJ/cm^2 per pulse. The number at the right represents the experimental event number. The data shown in Fig.6b is the average obtained from the measurements 1-6.

metallic films is given by the Walker limit[26] and is on the order of 100 ms, then in order to displace a DW over a distance of $\sim$50 nm one needs 0.5 ns. This suggests that the displacement of the DW proceeds for much longer than the optical pulse duration. Hence, a displacement solely due to the opto-magnetic field via the IFE[27] or ultrafast spin transfer torque[14] as reported[10,11,13,18] earlier is unlikely. L. Thomas et $al.$,[28] demonstrated that the DWs in permalloys propagate via inertial motion for longer than a nanosecond right after the external stimulus is removed. However, the inertial motion due to the diffusive magnons in Co/Pt is limited to 40 ps[29], which is still one order of magnitude shorter[30] than the one required to describe our observations.

There are several microscopic mechanisms[31–33] with temperature-induced domain wall motion have been reported. These mechanisms are based on the existence of thermal gradients between areas with oppositely oriented magnetizations. Due to magnetic circular dichroism, there will be differential absorption[34] of given circularly polarized pulses by the $M^\downarrow$ and $M^\uparrow$-regions. This different absorption is of the order of 1.5 %, obtained from reflectivity signals(see Fig.8b), resulting in a temperature gradient from the low-absorbing domain to the high-absorbing domain over a distance comparable to the width of the DW. The lifetime of this thermal gradient is related to heat diffusion and will be much longer than the initial optical pulse. This value can be esti-

mated from the magnetization recovery time, which is longer than 0.5 ns (see Fig. 2b). This value is of the same order of magnitude as estimated for the helicity dependent driving mechanism of DWs as observed in our Co/Pt multilayers. Since the DW energy decreases with increasing temperature there is a thermodynamic driving energy towards the hotter region to lower the DW energy[33]. Further, using micromagnetic approach via Landau-Lifshitz-Bloch (LLB) equation of motion, Hinzke and Nowak,[33] predicted that temperature gradients in a ferromagnetic nanowire cause a DW motion also arising from a magnonic spin Seebeck effect. We analyze our DW displacement results in light of these findings
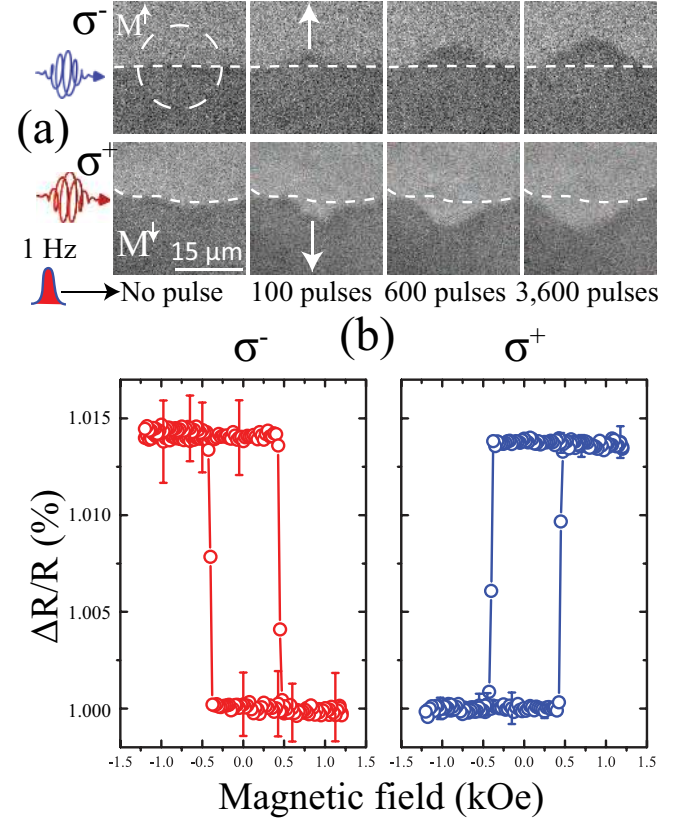

Figure 8. (a) (top) Magneto-optical images of laser-induced domain wall displacement region separating $M^\downarrow$ and $M^\uparrow$-domains, when subjected to the repetitive action of the σ^--pump pulses at the center of dashed circle. The repetition rate is 1 Hz. The pump fluence is 0.4 mJ/cm^2, the pulse duration is 4.0 ps. (bottom) Same as (top) but for the case of σ^+-pump pulse pulses. We have used dashed curves to show the initial position of the DW. Note that the direction of displacement of the DW is controlled with the helicity of the laser pulses. (b) Reflected intensity signals, off the sample surface, of σ^- (left) and σ^+ (right) circularly polarized laser plotted as a function of applied magnetic field. The light used is a continuous wave He:Ne laser with an emission wavelength at 633 nm. Note that similar results are obtained when the incident light is replaced with a 100 fs, 1 kHz repetition laser at a wavelength of 800 nm.

assuming that due to differential absorption of a σ-laser pulse, there exists a temperature gradient across the DW. A magnonic spin current that drives the magnons from hotter to colder regimes. However, due to conservation of angular momentum, this spin current drags the DW towards hotter region. The DW slides without any precession until the walker breakdown limit is reached. The velocity of this sliding is given by the temperature gradient across the DW. As reported in Ref.33, the DW in a ferromagnetic nanowire with a damping constant (α) of 0.1, displaces about 45 nm within 1 ns. However, the sliding of the DW due to thermal gradient is strongly dependent on the value of α. Since this value for our samples is very similar[29] to what has been reported in Ref.33, we can safely compare the thermal gradient driven DW displacement values, and are in good agreement with our laser-induced DW displacements. Assuming a 1 K difference in temperature after optical excitation this would result in a 0.2 K/nm across a 5 nm DW.

While there is not qualitative difference in the reversal behavior with P, within the error bars in our statistics the experiments with $P \leq 0.01$ s requires a somewhat larger number of pulses reverse the magnetization (Fig. 5). This difference suggests that there is a modest accumulation of heat in the sample that has been observed in similar experiment with high repetition rate optical excitations[22]. This results in reducing the overall net magnetization in the laser-exposed region. As a result of which the temperature gradient created across the DW will be lower than what it should be in the case of higher P values. Hence, the laser-induced displacement of the DW becomes ineffective and requires a larger number of pump pulse before the size of the laser-induced reversed domain reaches its equilibrium value. This is consistent with the laser conditions determined from the P = 0.002 s case presented in Fig.1.

The pulse length dependence study clearly revealed the lattice temperature is the most dominant one in determining the initial demagnetization induced by the laser pulses. The timescale of a few picoseconds suggests that the electron-phonon interaction, responsible for equilibrating the electron and lattice temperatures, plays an important role. However, we still have to understand why multi-pulse excitation with either longer pulses with slightly higher fluencies or shorter pulses with slightly lower fluencies cannot switch but only induce a multi-domain pattern still remains to be answered.

In conclusion, we have experimentally determined the multi-scale spatial and temporal processes of helicity-dependent all-optical switching in ferromagnetic Co/Pt multilayers. We successfully demonstrated that the magnetic switching is multi-pulsed in nature. Since submission of this manuscript there have been several recent reports and are in good agreement with our findings[16,37–39]. We also showed that the multi-pulse switching, in ferromagnetic thin-films, proceeds via thermally-induced stochastic nucleation of reversed domains followed by a helicity-dependent deterministic growth via DW motion. By varying the delay between pump pulses, we further identified the regime, pulse repetition-rate$\geq$100 Hz, where heat accumulation affects the growth of the reversed magnetic domains. The controllability over the direction of the DW displacement from the nucleation sites is the key element of the growth process. We revealed that during the initial helicity-dependent growth, a single pump pulse results in a DW displacement of 50 nm. This suggests that during the initial growth regime the DW is most likely driven by the thermal gradient which emerges due to the significant value of magnetic circular dichroism in these Co/Pt multilayers.

* rmedapalli@ucsd.edu

[1] E. Beaurepaire, J.-C. Merle, A. Daunois, and J.-Y. Bigot, Phys. Rev. Lett. **76**, 4250 (1996).

[2] A. Kirilyuk, A. V. Kimel, and Th. Rasing, Rev. Mod. Phys., **82**, 2731-2784 (2010).

[3] M. Savoini, R. Medapalli, B. Koene, A. R. Khorsand, L. Le Guyader, L. Duò, M. Finazzi, A. Tsukamoto, A. Itoh, F. Nolting, A. Kirilyuk, A. V. Kimel, and Th. Rasing, Phys. Rev. B **86**, 140404(R) 2012.

[4] T. Kampfrath, A. Sell, G. Klatt, A. Pashkin, S. Mährlein, Th. Dekorsy, M. Wolf, M. Fiebig, A. Leitenstorfer and R. Huber, Nature Photon. **5**, 31-34 (2011).

[5] F. Hellman, A. Hoffmann, G. S. D. Beach, E. E. Fullerton, Ch. Leighton, A. H. MacDonald, D. A. Arena, H. A. Dürr, P. Fischer, J. Grollier, J. P. H. Tomas Jungwirth, A. V. Kimel, B. Koopmans, I. N. Krivorotov, A. K. Petford-Long, James M. Rondinelli, N. Samarth, I. K. Schuller, A. N. Slavin, M. D. Stiles, A. Thiaville, and B. L. Zink, Rev. Mod. Phys. **89**, 025006 (2017).

[6] C.-H. Lambert, S. Mangin, B. S. D. Ch. S. Varaprasad, Y. K. Takahashi, M. Hehn, M. Cinchetti, G. Malinowski, K. Hono, Y. Fainman, M. Aeschlimann, and E. E. Fullerton, Science **345**, 1337-1340 (2014).

[7] T. A. Ostler, J. Barker, R. F. L. Evans, R. W. Chantrell,

U. Atxitia, O. Chubykalo-Fesenko, S. El Moussaoui, L. Le Guyader, E. Mengotti, L.J. Heyderman, F. Nolting, A. Tsukamoto, A. Itoh, D. Afanasiev, B.A. Ivanov, A.M. Kalashnikova, K. Vahaplar, J. Mentink, A. Kirilyuk, Th. Rasing, and A.V. Kimel, Nature Communications **3**, 666 (2012).

[8] J. H. Mentink, J. Hellsvik, D. V. Afanasiev, B. A. Ivanov, A. Kirilyuk, A. V. Kimel, O. Eriksson, M. I. Katsnelson, and Th. Rasing, Phys. Rev. Lett. **108**, 057202 (2012).

[9] M. O. A. Ellis, E. E. Fullerton, and R. W Chantrell, Scientific Reports **6**, 30522 (2016).

[10] R. John, M. Berritta, D. Hinzke, C. Müller, T. Santos, H. Ulrichs, P. Nieves, J. Walowski, R. Mondal, O. Chubykalo-Fesenko, J. McCord, P. M. Oppeneer, U. Nowak, and M. Münzenberg, Scientific Reports **7**, 4114 (2017).

[11] P. Nieves and O. Chubykalo-Fesenko, Phys. Rev. Applied 5, 014006 (2016).

[12] Y. K. Takahashi, R. Medapalli, S. Kasai, J. Wang, K. Ishioka, S. H. Wee, O. Hellwig, K. Hono, and E. E. Fullerton, Phys. Rev. Applied **6**, 054004 (2016).

[13] T. D. Cornelissen, R. Córdoba, and B. Koopmans, Appl. Phys. Lett. **108**, 142405 (2016).

[14] F. Freimuth, S. Blügel, and Y. Mokrousov, Phy. Rev. **B 94**, 144432 (2016).

[15] J. Gorchon, Y. Yang, and J. Bokor, Phys. Rev. B **94**, 020409(R) (2016).

[16] M. S. El Hadri, P. Pirro, C.-H. Lambert, S. Petit-Watelot, Y. Quessab, M. Hehn, F. Montaigne, G. Malinowski, and S. Mangin, Phys. Rev. B **94**, 064412 (2016).

[17] K. Vahaplar, A. M. Kalashnikova, A.V. Kimel, D. Hinzke, U. Nowak, R. Chantrell, A. Tsukamoto, A. Itoh, A. Kirilyuk, and Th. Rasing, Phys. Rev. Lett. **103**, 117201 (2009).

[18] K. Vahaplar, A. M. Kalashnikova, A. V. Kimel, S. Gerlach, D. Hinzke, U. Nowak, R. Chantrell, A. Tsukamoto, A. Itoh, A. Kirilyuk, and Th. Rasing, Phys. Rev. B **85**, 104402 (2012).

[19] Y. Hashimoto, A. R. Khorsand, M. Savoini, B. Koene, D. Bossini, A. Tsukamoto, A. Itoh, Y. Ohtsuka, K. Aoshima, A. V. Kimel, A. Kirilyuk, and Th. Rasing, Rev. Sci. Inst. **85**, 063702 (2014).

[20] S. Alebrand, M. Gottwald, M. Hehn, D. Steil, M. Cinchetti, D. Lacour, E. E. Fullerton, M. Aeschlimann, and S. Mangin, App. Phys. Lett. 101, 164208 (2012).

[21] M. Djordjevic, and M. Münzenberg Phys. Rev. B **75**, 012404 (2007).

[22] A Hassdenteufel, C Schubert, P Reinhardt, P Richter, M Fronk, D R T Zahn, R Bratschitsch3 G Salvan, and M Albrecht, Optics Express 22(8) 10017-10025 (2014)

[23] K. Binder, Theory of first-order phase transitions, Reports on progress in physics, vol. 50, no. 7, p. 783, 1987.

[24] E. Beaurepaire, M. Maret, V. Halté, J.-C. Merle, A. Daunois, and J.-Y. Bigot, Phys. Rev. B **58**, 12134 (1998).

[25] J. Pommier, P. Meyer, G. Pénissard, and J. Ferré, P. Bruno, and D. Renard Phys. Rev. Lett. **65**, 2054 (1990).

[26] P. J. Metaxas, J. P. Jamet, A. Mougin, M. Cormier, J. Ferré, V. Baltz, B. Rodmacq, B. Dieny, and R. L. Stamps, Phys. Rev. Lett. **99**, 217208 (2007).

[27] A. V. Kimel, A. Kirilyuk, P. A. Usachev, R. V. Pisarev, A. M. Balbashov, and Th. Rasing, Nature (London) **435**, 655(2005).

[28] L. Thomas, R. Moriya, Ch. Rettner, S. S. P. Parkin, Science **330**, 1810 (2010).

[29] A. Barman, S. Wang, O. Hellwig, A. Berger, E. E. Fullerton, and H. Schmidt, Journal of Applied Phys. **101**, 09D102 (2007).

[30] A. Ganguly, S. Azzawi, S. Saha, J. A. King, R. M. Rowan-Robinson, A. T. Hindmarch, J. Sinha, D. Atkinson, and A. Barman, Scientific Reports **5**, 17596 (2015).

[31] A. J. Ramsay, P. E. Roy, J. A. Haigh, R. M. Otxoa, A. C. Irvine, T. Janda, R. P. Campion, B. L. Gallagher, and J. Wunderlich1, Phys. Rev. Lett. **114**, 067202 (2015).

[32] W. Jiang, P. Upadhyaya, Y. Fan, J. Zhao, M. Wang, Li-Te Chang, M. Lang, K. L. Wong, M. Lewis, Y.-Ting Lin, J. Tang, S. Cherepov, X. Zhou, Y. Tserkovnyak, R. N. Schwartz, and K. L. Wang, Phys. Rev. Lett. **110**, 177202 (2013).

[33] D. Hinzke, and U. Nowak, Phys. Rev. Lett. **107**, 027205 (2011).

[34] A. R. Khorsand, M. Savoini, A. Kirilyuk, A.V. Kimel, A. Tsukamoto, A. Itoh, and Th. Rasing, Phys. Rev. Lett. **108**, 127205 (2012).

[35] J H Franken, M Hoeijmakers, R Lavrijsen, and H J M Swagten, J. Phys.: Condens. Matter **24**, 024216 (2012).

[36] A. Fognini, G. Salvatella, and R. Gort, Structural Dynamics **2**, 024501 (2015).

[37] F Hoveyda, E Hohenstein, and S Smadici, J. Phys.: Condens. Matter **29**, 225801 (2017).

[38] F. Cheng, Dissertation thesis, November 2016, Northeastern University Boston, Massachusetts.

[39] Yu. Tsema, G. Kichin, O. Hellwig, V. Mehta, A. V. Kimel, A. Kirilyuk, and Th. Rasing, Appl. Phys. Lett. **109**, 072405 (2016).